# Selector devices for x-point memory

10

*Jeonghwan Song, Yunmo Koo, Jaehyuk Park, Seokjae Lim, Hyunsang Hwang*
Department of Materials Science and Engineering, Pohang University of Science and Technology, Pohang, South Korea

## 10.1 Introduction

Crossbar arrays capable of implementing device cross sections of ~$4F^2$ have been studied for ultrahigh-density storage architectures, where $F$ is the minimum feature size of the array [1]. For this purpose, two-terminal emerging memory devices such as phase change memory (PCM) [2] and resistive RAM (RRAM) [3] have been proposed in storage devices. To operate the storage device in the crossbar array, different voltages are applied to the line edges of the row and column where the *selected cell* is located, which causes a *net voltage drop* in the selected cell. When the net voltage drop is greater than the threshold voltage of the storage device, the data states change through the program/erase process. On the other hand, under low-voltage state, the stored data states can be read without change of data.

However, the crossbar array architecture has inevitable problems such as undesired current flow and data disturbance due to a nonzero net voltage drop in *half-selected cells* located in the same column or row line as the selected cells and *unselected cells* near the selected cell. Undesired current flow such as leakage and sneak path currents that can occur in both the unselected and the half-selected cells during the read operation degrades the sense margin of the crossbar array. In addition, the data disturbance is a critical problem that can cause data loss due to the high net voltage in the half-selected cells during the program/erase process.

Therefore, an access device called a *selector device* is required to cause the desired net voltage drop only in the selected cells in crossbar array [4]. The selector device, which acts as a switch, is turned on when a voltage above a threshold value is applied that leads to increase in the net voltage drop to the storage device. However, in the low-voltage regime, the off state is maintained, which suppresses in undesired current flow and data disturbance.

To achieve this goal, the selector device has lots of requirements in the electrical characteristics and device fabrication process. Among them, the extremely low OFF current ($I_{OFF}$) characteristic is the most important parameter that can increase in the sensing margin of crossbar array. On the other hand, the ON-current density must be high enough so that there is no limit on the required current during programming/erasing of the storage device. Thus, the selector device should have highly nonlinear *I-V* characteristics. Other requirements include fast switching speeds, infinite cycling endurance, excellent device uniformity, large voltage margins (voltage window

**Advances in Non-volatile Memory and Storage Technology. https://doi.org/10.1016/B978-0-08-102584-0.00011-5**

separating the ON and OFF states), compatible operating voltage conditions with storage devices, low-temperature fabrication processes, high thermal stability, 3D stackable, and two-terminal device structure. CMOS transistors are the best selector devices with the required electrical characteristics, but the three-terminal device architecture is not suitable for ultrahigh-density crossbar array architectures. In addition, the P-N diodes rectifying the current flow are limited in use due to the high-temperature process conditions. Therefore, various selector devices have been suggested based on a new operating mechanisms to meet the criteria for the selector device such as mixed ionic electronic conduction (MIEC) device, tunnel barrier type device, insulator-metal transition (IMT), Ovonic threshold switching (OTS), and conductive-bridging RAM (CBRAM)-type selector device.

Among them, this chapter introduces *threshold-type* selector devices, such as IMT, OTS, and CBRAM-type, which have the potential for atomic scale scalability, and discusses about the guidelines for future development of selector devices.

## 10.2 Insulator-metal-transition selector

Certain transition metal oxide such as NiO, $VO_2$ [5], and $NbO_2$ [6] are highlighted thanks to the special properties that change from an insulating state to a metallic state under certain conditions such as a specific temperature [7], optical excitation [8], or an electric field [9]. These materials change conductivity by rearranging their crystal structure at critical temperature called Mott-Peierls transition, which is shown in Fig. 10.1 [10, 11].

Recently, electrically driven IMT (E-IMT) devices suggested as a selector device which has bidirectional threshold characteristics for ReRAM x-point applications thanks to their simple metal/insulator/metal structure and fast transition speed. M. Son et al. suggested the $VO_2$-based threshold switch device as a selector [12] as shown in Fig. 10.2.

When the applied voltage on $VO_2$ device exceeds a critical voltage called threshold voltage ($V_{th}$), the device changes its state from insulating state to metallic state. The transition mechanism of $VO_2$ is usually interpreted as the result of joule heating by electric field. As shown in Fig. 10.1A, the $VO_2$ changes its state at about 340 K. When a voltage is applied to the $VO_2$ device, joule heating occurs due to the current flowing through the material. When the temperature rising due to joule-heating exceeds 340 K on the $VO_2$ device, the $VO_2$ material changes to a metallic state. Actually, S. Kumar showed $VO_2$ changes from an insulating state to a metallic state when the internal temperature exceeds 340 K due to joule heating (Fig. 10.3A) [13]. However, $VO_2$-based selector has limitations as a selector because their transition temperature (~340 K, Fig. 10.3B) is too close to room temperature (RT) [14], reducing control precision in circuit. For replacement, some groups suggested the $NbO_2$-based selector device which has high transition temperature (1080 K, Fig. 10.3C) [15, 16].

In their research, ultrathin $NbO_2$ film was fabricated by reactive sputtering method and patterned to nanoscale device. Similar to $VO_2$ device, the $NbO_2$ selector

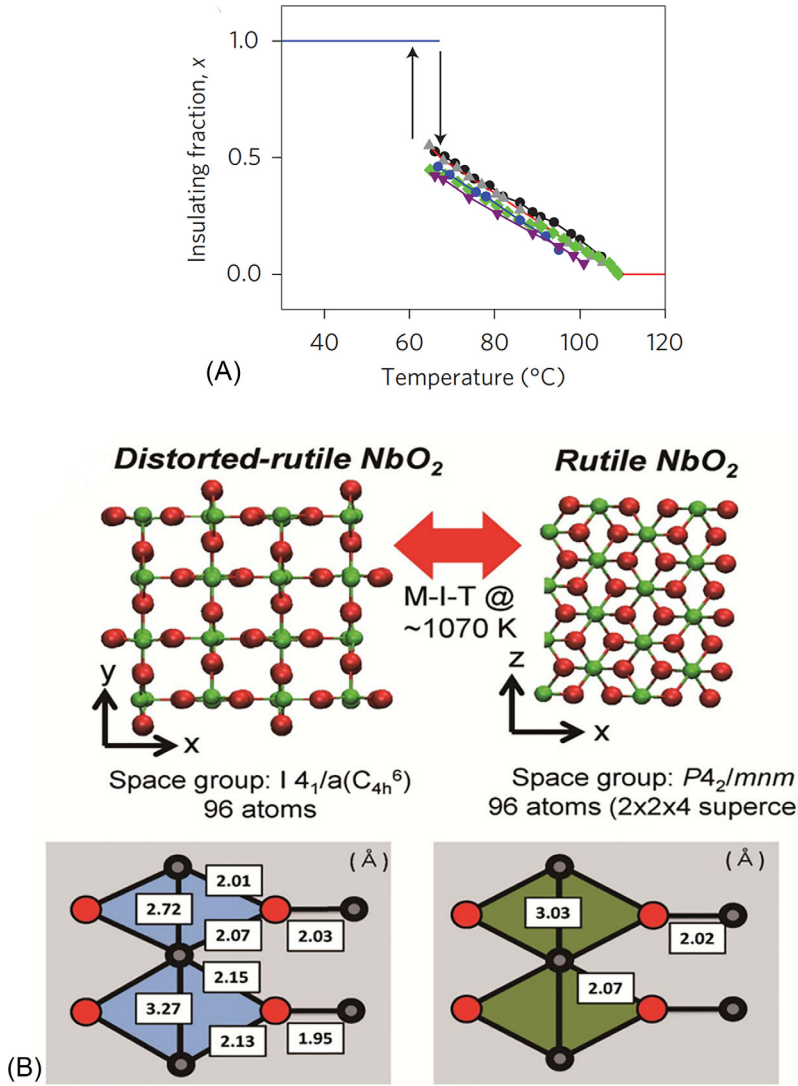


**Fig. 10.1** (A) IMT characteristic according to temperature in $VO_2$ [10]. (B) IMT characteristics in $NbO_2$ [11].

exhibits repeatable threshold characteristics over 1000 switching cycles (Fig. 10.3C and D) [15]. Moreover, $NbO_2$ device has additional unique characteristics as a selector such as fast transition speed (<50 ns) and high thermal stability (>430 K). E. Cha et al. also announced that the device characteristics such as forming voltage ($V_F$), $V_{th}$, and $I_{OFF}$ can be controlled by thickness and device area engineering by using TiN/$NbO_2$/W device [17]. According to their research, the $V_{th}$ can be reduced by the thickness of $NbO_2$ layer and the $I_{OFF}$ can be reduced by reducing the device size as shown in Fig. 10.4. Thanks to controllability of the $NbO_2$ device, it is easy to

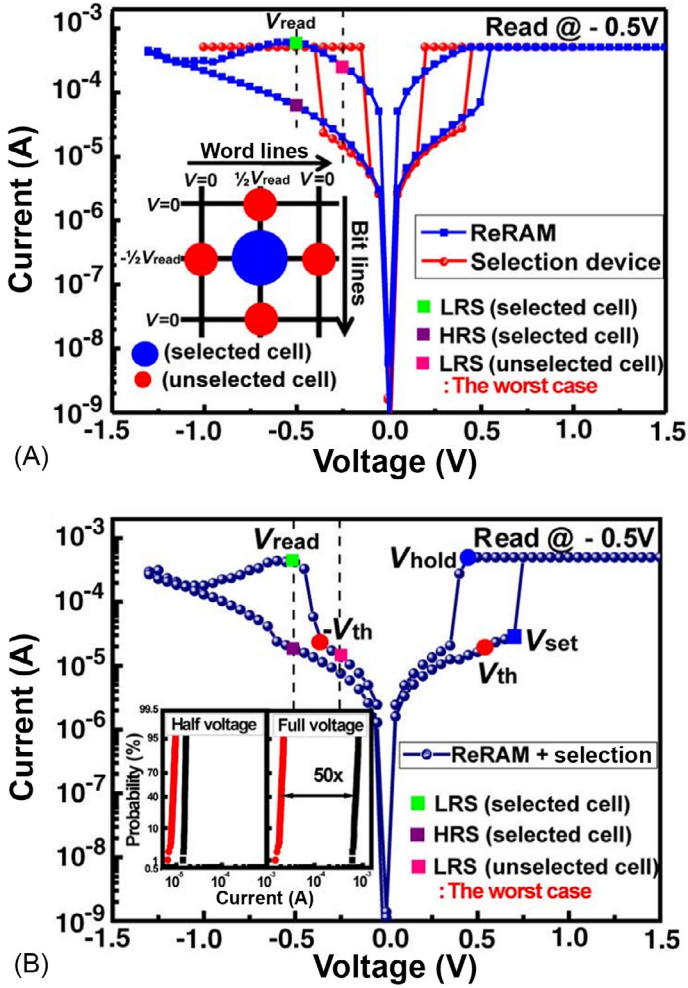


**Fig. 10.2** (A) *I-V* characteristics of $VO_2$ selector device and ReRAM device and (B) the *I-V* characteristics of 1S1R structure [12].

fabricate $NbO_2$ device which has proper device characteristics with variety ReRAM devices for 1S1R structure.

Later, in order to develop the $NbO_2$ device through a more accurate analysis, many groups studied the mechanism of the E-IMT phenomenon of $NbO_2$ device like $VO_2$ device. Many groups initially attempted to interpret the E-IMT of $NbO_2$ as a result of joule heating just as $VO_2$ [18]. However, the joule-heating model conflicts with the fact that transition temperature of $NbO_2$ (1080 K) is much higher than the temperature that can be induced by Joule heating of the insulating state of $NbO_2$ [19]. For more accurate mechanism analysis, a number of groups tried to show that $NbO_2$ can change its resistance far below the IMT temperature of $NbO_2$

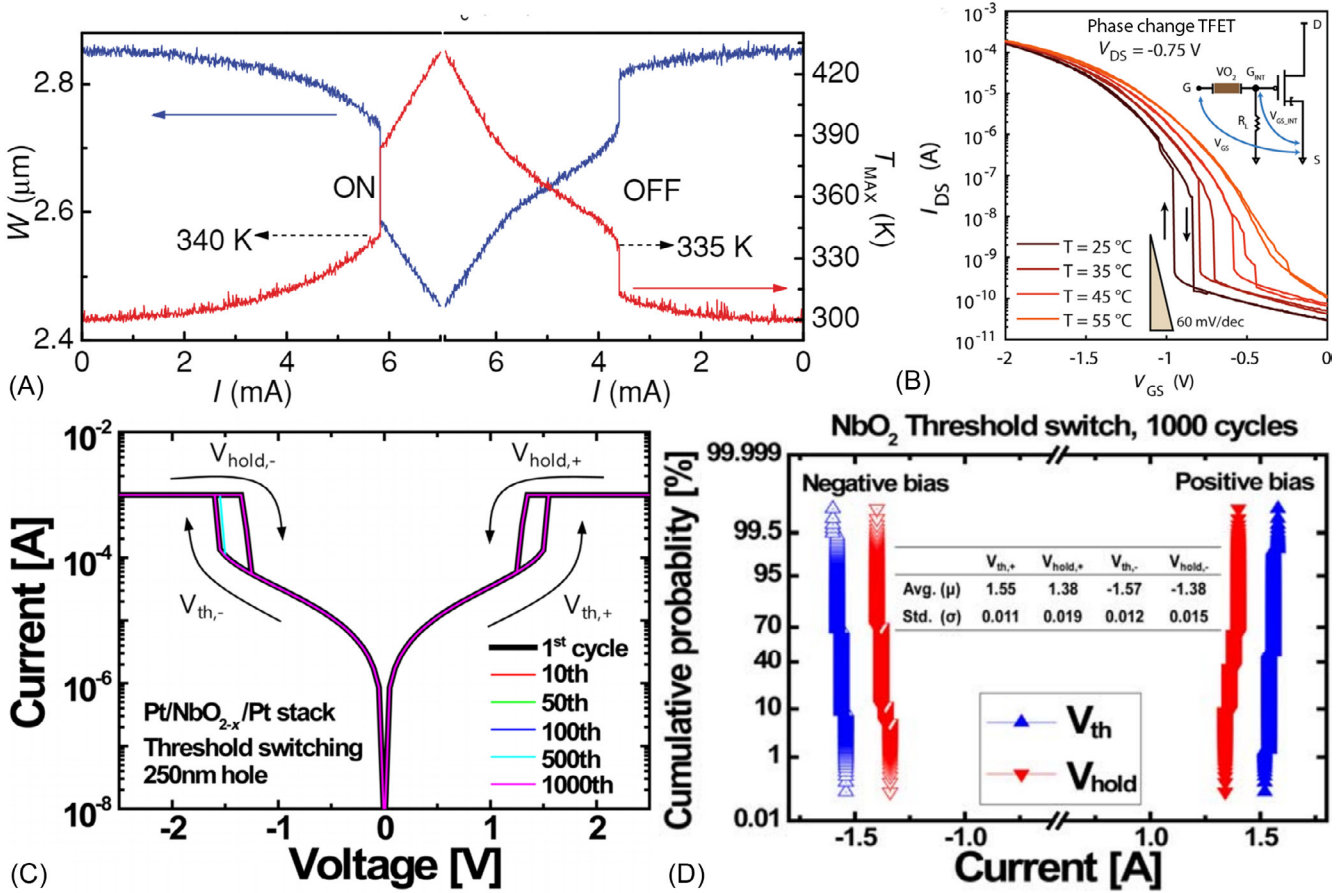


**Fig. 10.3** (A) The temperature of $VO_2$ film under electrical field *(red)* and *(blue)* [13]. (B) The *I-V* characteristics of $VO_2$ device shows that it cannot act as selector at over 340 K [14]. (C) The *I-V* characteristics of IMT behavior of Pt/$NbO_2$/Pt devices. (D) Distribution of $V_{th}$ and $V_{hold}$ of Pt/$NbO_2$/Pt device during 1000 cycles [15].

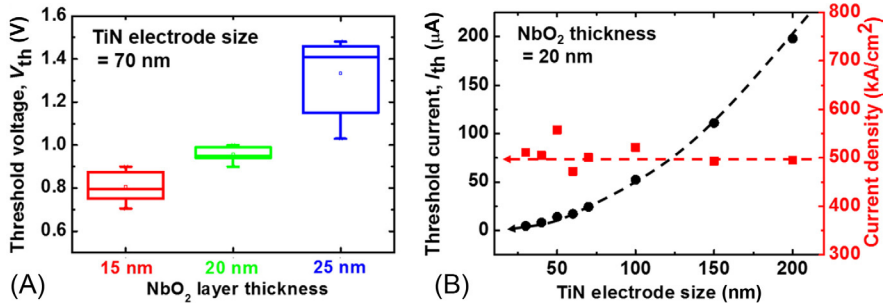


**Fig. 10.4** (A) Distribution of $V_{th}$ and (B) $I_{th}$ ($I_{OFF}$) of TiN/$NbO_2$/W devices according to thickness and size of $NbO_2$ layer. $V_{th}$ decreases as thickness of $NbO_2$ layer decreases, and $I_{th}$ decreases as device size of $NbO_2$ decrease [17].

(1080 K) based on thermal runaway model with Poole-Frenkel simulation [20–22]. According to Funck C. et al.'s description, they claim that IMT can be started at much lower temperatures than the original transition temperature of $NbO_2$ (1080 K) because of combination of barrier lowering by electrical field and joule-heating effect as shown in Fig. 10.5A [20]. Actually, the simulation result (Fig. 10.5) shows that the temperature of starting point of transition is almost 320 K which is much lower temperature than original transition temperature of $NbO_2$, and the temperature and conductivity can self-accelerated until reach to the metallic state by their thermal-runaway model.

Similarly, J. Park et al. adopted the field-induced nucleation theory to clarify the mechanism of $NbO_2$ E-IMT by measuring the delay time of the film at various temperature and voltage [23]. Despite mechanism analysis and various attempts to improve the performance of IMT selectors, the $I_{OFF}$ of the IMT selector is relatively high compare with other selector candidates such as CBRAM-type selectors and OTS selectors. To reveal the origin of leakage current of IMT devices, some groups try to C-AFM analysis to find the leakage point of the film [24, 25].

Fig. 10.6 shows that the that the local amorphous state in polycrystalline thin-film and the grain boundaries can cause leakage current, especially with large defect density [24, 25]. These defects generate the conduction subbands between conduction band and valance band of IMT materials ($NbO_2$, $VO_2$) and these generate the leakage current. Moreover, the interface defects between electrode and IMT materials also can generate the leakage current because the defects can pin the Schottky barrier height and it can not be formed perfectly [26]. To passivate the defects and reduce the leakage current, many groups tried to insert the barrier structure which can eliminate both of interfacial and bulk defects [24, 26, 27].

X. Liu et al. insert a thin $HfO_x$ layer between bottom electrode and $NbO_2$ IMT layer which forms the narrow conductive filament during forming process. During their research, the most of defects of the $NbO_2$ film are suppressed and a low $I_{OFF}$ can be obtained compared with the single $NbO_2$ device since the other $HfO_x$ portions without a conductive filament are in a very high resistance state, as shown in Fig. 10.7A and B. Similarly, J. Park et al. also inserted the $NiO_y$ barrier layer in both

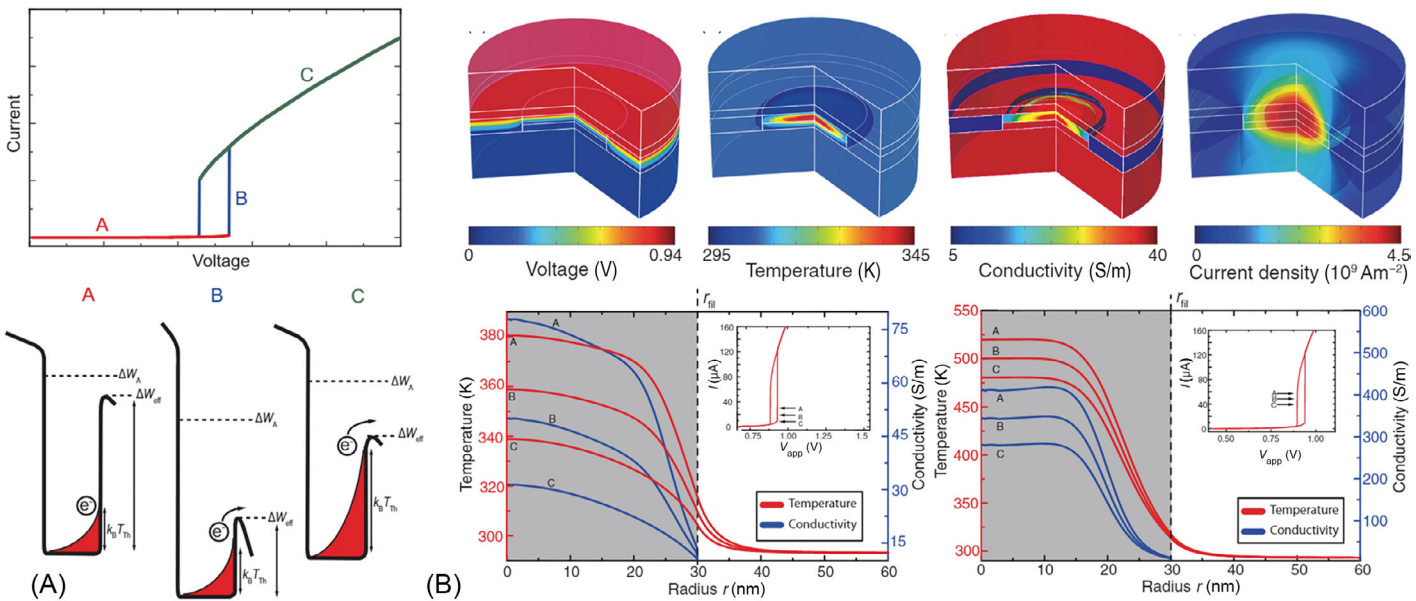


**Fig. 10.5** (A) Schematic diagram of the energy barrier to transit to a metallic state from an insulating state of the $NbO_2$ device. In process A, the device cannot change because of insufficient energy to transition. In process B and C, the device can change its state due to a combination of joule-heating induced thermal energy and energy barrier lowering by an electrical field. (B) A thermal simulation of a $NbO_2$ device during operation shows that the transition can occur much lower temperature (~320 K) than the transition temperature of the $NbO_2$ device (~1070 K) under an electrical field [20].

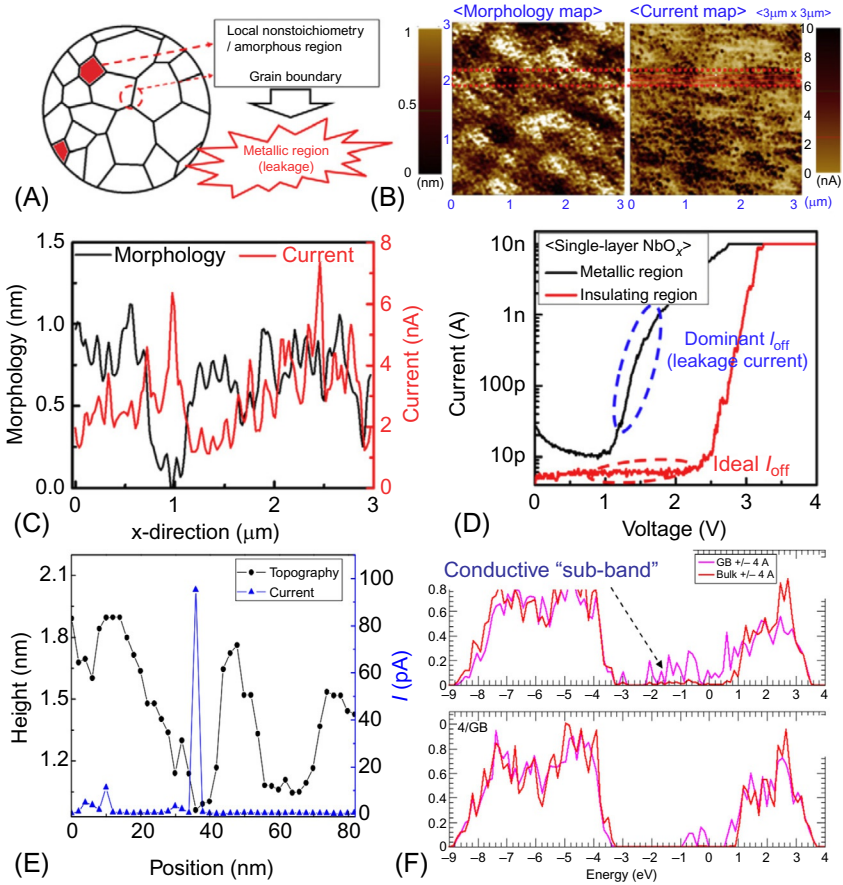


**Fig. 10.6** (A) The schematic diagram of leakage source of $NbO_2$ film. (B) The morphology and current map of the $NbO_2$ film, and (C-D) line and point profiles *(red box in (B))* show that the morphologically shrink position which corresponding to defects generate the leakage current [24]. (E) Also the current map of $HfO_2$ device shows similar result of $NbO_2$ device. (F) The defects in IMT materials generate the conductive subband between valance band and conduction band [25].

side of between electrode and $NbO_2$ IMT layer ($W/NiO_y/NbO_2/NiO_y/W$) to form the perfect Schottky barrier height which can reduce the $I_{OFF}$ of $NbO_2$-based IMT device (Fig. 10.7C).

Additionally, suggested $NbO_2$-based selector by J. Park et al. also shows excellent characteristics as a selector devices such as high $I_{ON}/I_{OFF}$ ratio (>5400), high operating temperature (>453 K), fast transition speed (<2 ns), and drift-free operation as shown in Fig. 10.8. Due to the excellent selector characteristics of suggested $NiO_y$ inserted $NbO_2$ IMT device, they also can show a significantly improved readout margin (up to $2^9$ word lines) is possible in a large x-point memory array [26].

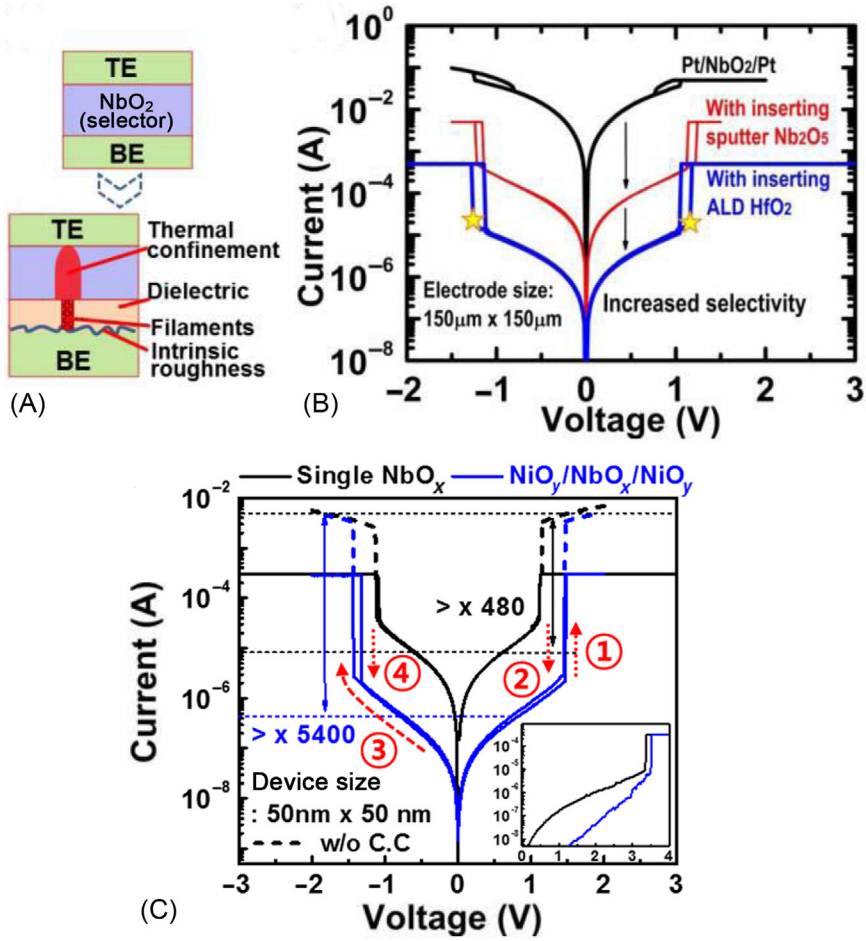


**Fig. 10.7** (A–B) The *I-V* characteristics of barrier inserted Pt/$HfO_2$/$NbO_2$/Pt device [27]. (C) W/$NiO_y$/$NbO_2$/$NiO_y$/W device. $I_{OFF}$ of both devices shows reduced $I_{OFF}$ compare with single layer $NbO_2$ device [26].

## 10.3 Ovonic threshold switching

OTS phenomenon is a field-dependent volatile threshold switching (TS) occurring in amorphous chalcogenide alloys, first reported by S.R. Ovshinsky in 1968 [28]. Recently, various OTS selector devices fabricated on wafers with patterned nanoscale electrodes have been reported whose performances are illustrated in Fig. 10.9. The first distinguishing factor of OTS among various types of TS phenomena is that it has comprehensively superior properties satisfying the various requirements of selector requirements. OTS material is highly insulating in its "OFF" state (~ 20 GΩ at 0.2 V (Fig. 10.9A) [29]), effectively minimizing current

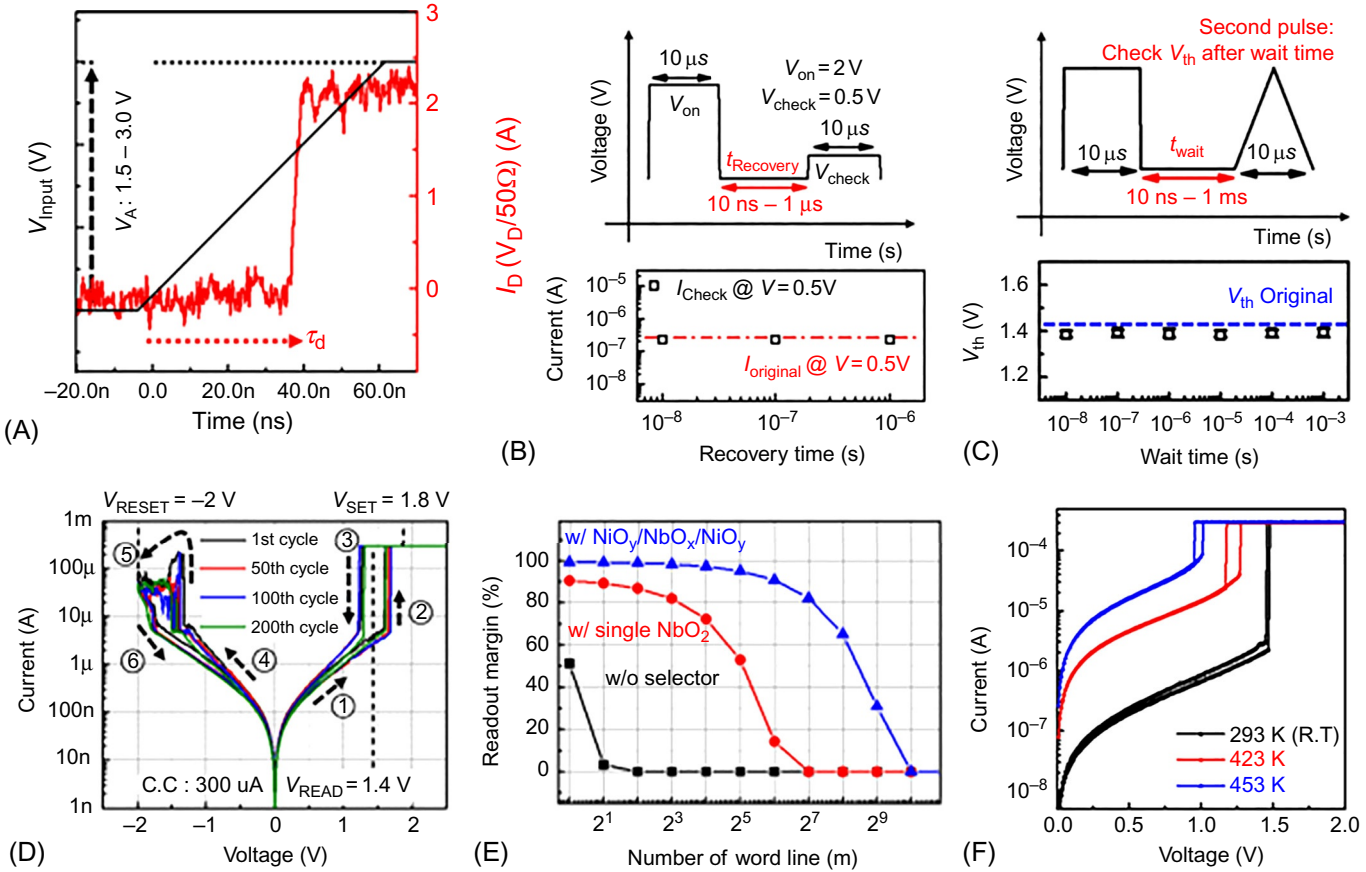


**Fig. 10.8** (A) The transition speed and delay time of W/$NiO_y$/$NbO_2$/$NiO_y$/W. The transition speed is under 2 ns and delay time is under 40 ns. (B) The recovery time test shows that the W/$NiO_y$/$NbO_2$/$NiO_y$/W device can recover its insulating state faster than 10 ns and (C) threshold voltage of the device is not changed by previous operation. (D) *I-V* characteristics of 1S1R structure which using W/$NiO_y$/$NbO_2$/$NiO_y$/W device as selector and (E) calculated read-out margin of cross-point array based on 1S1R result. (F) The W/$NiO_y$/$NbO_2$/$NiO_y$/W maintain threshold characteristics at above 453 K [26].

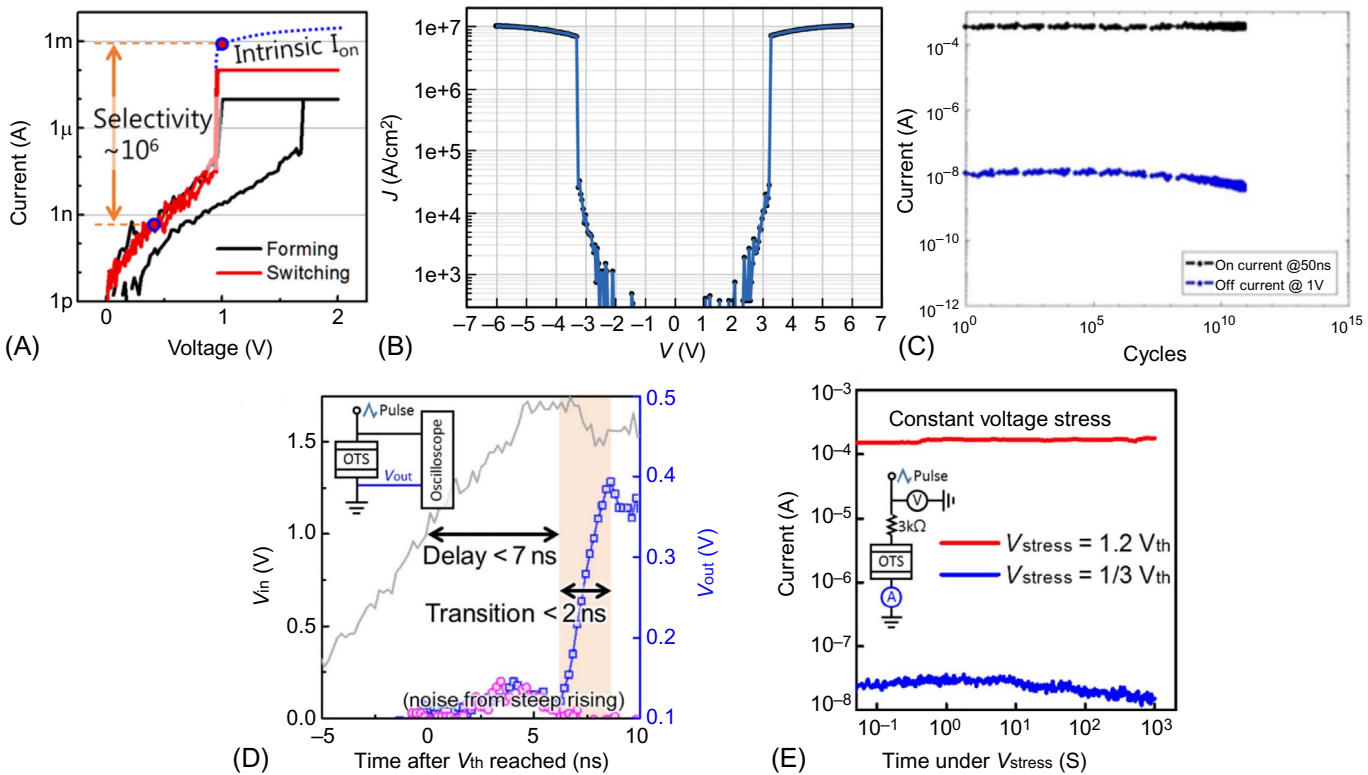


**Fig. 10.9** Reported performance of OTS selector devices.

flow through the device (30 MA/cm$^2$ (Fig. 10.9B) [30]). Once the external electric field exceeds the threshold voltage ($V_{th}$), OTS material exhibits a rapid and volatile resistance decrease and turns into its low resistance "ON" state (< 1 kΩ [29]) through "S"-shaped negative differential resistance change, allowing high current supply (> 1.1 × 10$^7$ A/cm$^2$ [31]) for memory operation. This resistance change in OTS material is nondestructive and repeatable (> 8 × 10$^{12}$ cycles (Fig. 10.9C) [32] and > 10$^{11}$ cycles [33]), instant (short delay time < 2 ns (Fig. 10.9D) [34]), fast (transition time < 5 ns [35]), abrupt (switching slope < 1 mV/dec [29]), thus suitable for selector device application. Electrical stress test results show that both ON and OFF states are electrically stable. Under more than 10$^3$ s of either constant current (300 μA [33]) or constant voltage (1.2 $V_{th}$ (Fig. 10.9E) [34]) stress, performances of OTS devices were securely maintained.

To explain the OTS phenomenon, various theoretical studies have been conducted. Representative schematics of the studies including thermally induced instability by A.C. Warren [36], Shockley-Read-Hall recombination with impact

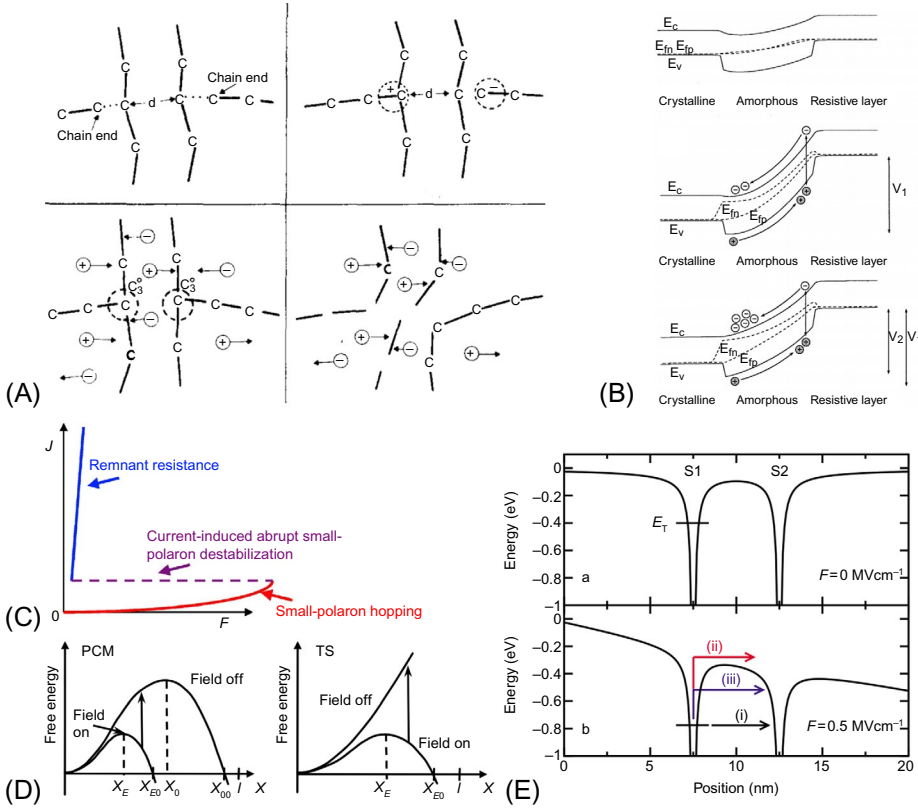


**Fig. 10.10** Various theoretical studies proposed to explain OTS phenomenon.

ionization by D. Adler (Fig. 10.10A) [37] and A. Pirovano (Fig. 10.10B) [38], polaron destabilization by D. Emin (Fig. 10.10C) [39], nucleation theory by M. Nardone (Fig. 10.10D) [40], and thermally assisted hopping model by D. Ielmini (Fig. 10.10E) [41]. Many of the above models explain the OTS as an electronic phenomenon with possible secondary thermal effects, suggesting the second distinguishing factor of OTS among various types of TS phenomena that it does not involve any atomic arrangements while switching [32]. Due to this advantage, OTS has a high potential in extremely fast operation speed [30, 34, 35], and superb cycling endurance ($> 8 \times 10^{12}$ cycles [32] and $> 10^{11}$ cycles [33]) among TS devices.

One drawback of OTS selector devices was its complex material (four to five elements for plausible device performance in usual [28, 31, 33, 36, 37]). However, recent reports showed that simple binary OTS materials such as GeTe, ZnTe, and SiTe could be showed even with improved selector device performances such as higher OFF resistance, lower ON resistance, faster operation speed, higher cycling endurance, and higher thermal stability (Fig. 10.11A) [29, 34]. However, to improve performances of the binary OTS devices further, many groups started to seek for new OTS materials and reported various OTS devices whose electrical properties are illustrated in Fig. 10.11. As a result, OTS has been reported in a number of chalcogenide materials (Fig. 10.11B–F) [28–37, 42–46]. While having Te or Se as a core element, the other components can be chosen from various species such as Ge, Si, P, As, Sb, Bi, Zn, or even N, B, or C. The freedom of choice of material combination greatly enhances the tenability of the OTS material [29, 32, 33, 42–46].

In recent OTS studies, it has become an important topic to improve thermal stability without sacrificing device performance. The thermal stability of various OTS devices reported in recent papers is illustrated in Fig. 10.12. To satisfy thermal budget of CMOS process, selector devices have to endurance temperature higher than 400°C but many of the reported OTS devices have shown performance degradation near 300°C (Fig. 10.12A and B) [33, 34, 42]. Consequently, approaches to investigate the performance degradation mechanism to improve the thermal stability have been actively carried out by field leading researches groups over the world (Fig. 10.12C) [33, 34, 42, 43]. Since, OTS material with high thermal stability withstanding 500°C annealing has already been reported (Fig. 10.12D and E) [31, 32], device scale high thermal stability would be hopefully achieved in the near future.

OTS is clearly one of the closest candidates to the commercialization of selector devices, but there are some important issues that are obviously need to be improved in advance. Analysis on device reliability issues such as cell-to-cell or cycle-to-cycle uniformity is not sufficient and needs further research. In addition, despite the fact that various different mechanisms have been suggested to explain the OTS behavior [32, 36–41, 43], a unified model is still missed. Therefore, a detailed study of the physics behind the OTS phenomena is needed to fully understand and tailor different electrical properties.

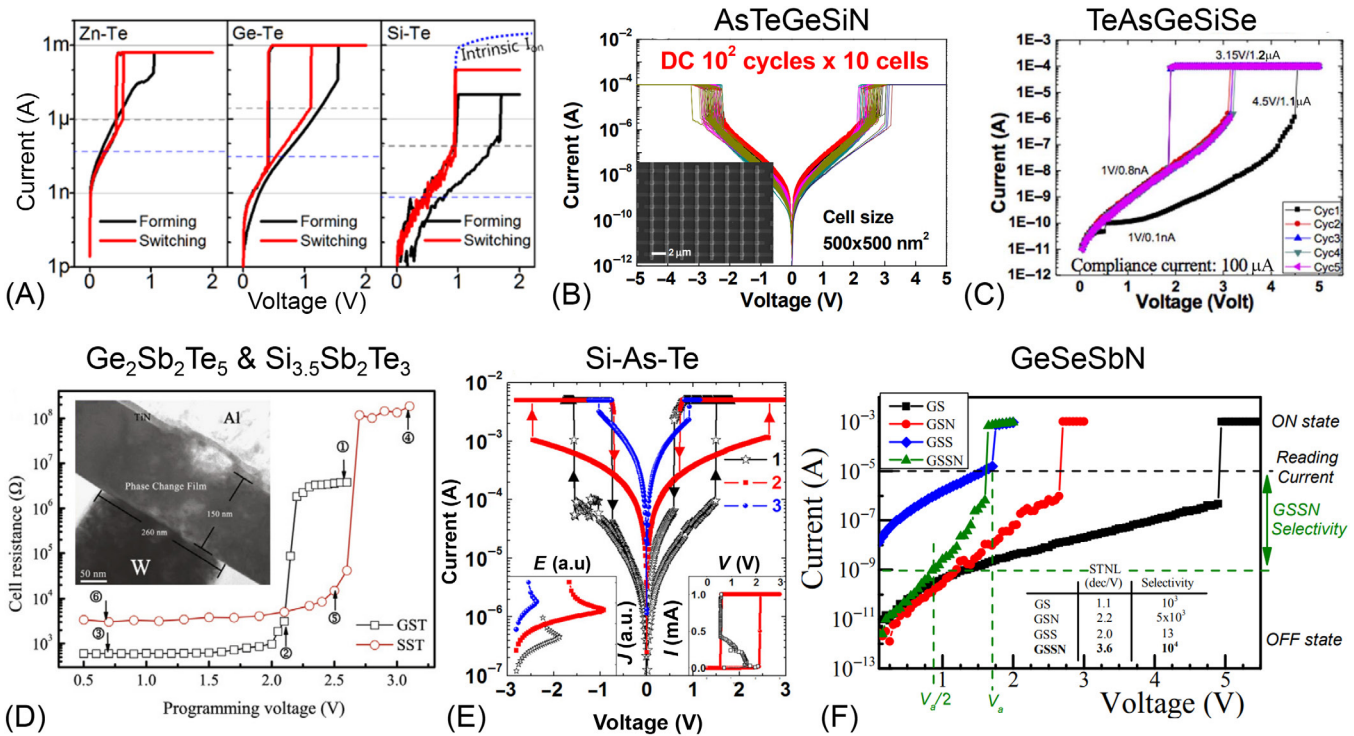


**Fig. 10.11** Diverse material pool of OTS devices enhances the tunability of their device properties.

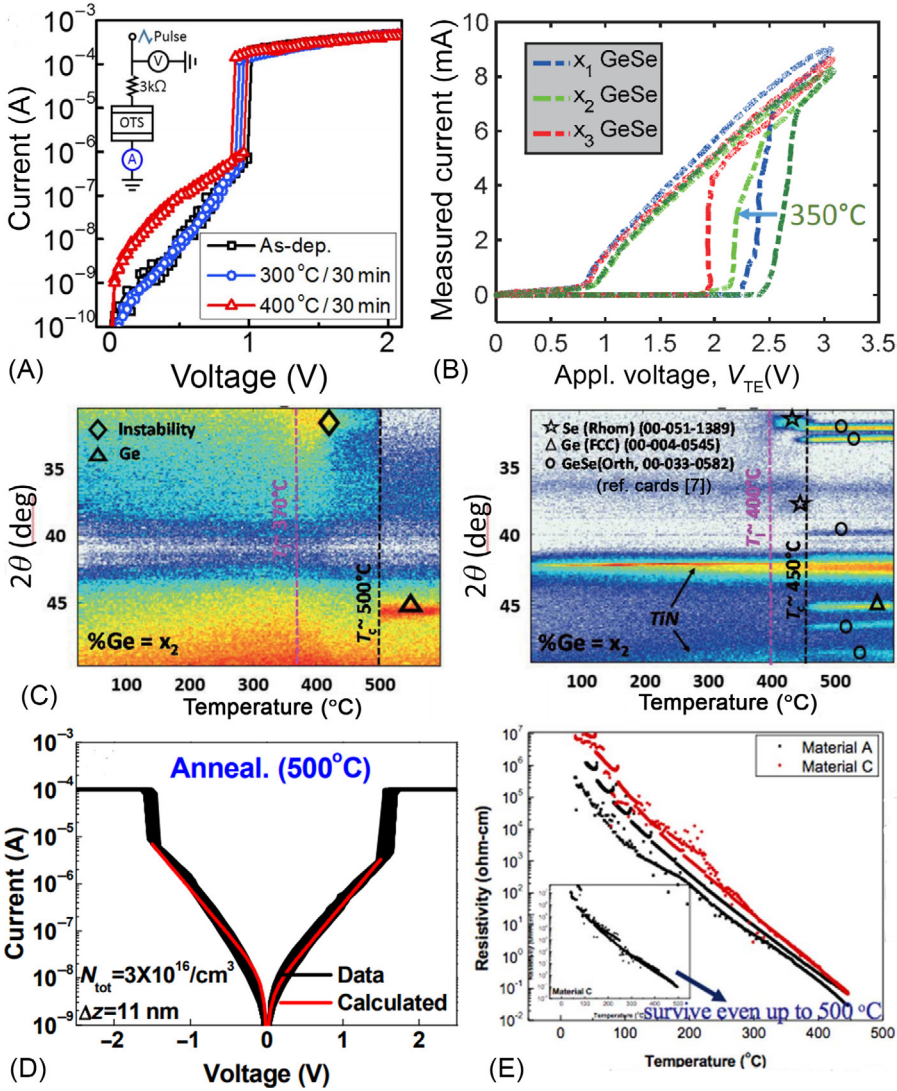


**Fig. 10.12** Thermal stability of OTS selector devices and studies to explain the device performance degradation in high temperature.

## 10.4 CBRAM-type selector

As a new approach, recently, there is growing interest in using instability of the filament in conventional conductive bridge random access memory (CBRAM) devices for selector applications. When the CBRAM device is programmed under a lower current compliance, the small and unstable Cu or Ag filament is formed. Accordingly, the spontaneous self-rupturing of the unstable filament is occurred when the applied bias

is removed which can be used as a TS devices. Various materials have been reported for the CBRAM-type TS device as a selector device [47–60].

Song et al. suggested the use of a Ag/Titanium oxide-based threshold switch ($Ag/TiO_2/Pt$) as a selector device in a crossbar array [55]. Fig. 10.13A shows the measured *I-V* characteristics. The $Ag/TiO_2/Pt$ device showed high selectivity (~$10^7$) and steep slope (<5 mV/dec). The exponential relation between time and voltage was also verified (Fig. 10.13B).

The Ag/amorphous Si-based devices (Ag/a-Si/Pt) were reported by the same group in Ref. [56]. A faster dissolution of the metal filament and lower down the $I_{OFF}$ were achieved by enhancing diffusivity of the Ag atoms and removing leakage paths in the a-Si film of the device through hydrogen doping of the a-Si layer.

Midya et al. reported Ag/Hafnium oxide-based ($Pd/Ag/HfO_x/Ag/Pd$) selector device [58]. The selector device exhibits a high selectivity of $10^{10}$, steep turn on slope of <1 mV/dec, and high endurance beyond $10^8$ cycles. They also demonstrated the vertical integration of $Pd/Ag/HfO_x/Ag/Pd$ threshold switch on top of a $Pd/Ta_2O_5/TaO_x/Pd$ memristor device. Fig. 10.14A shows a TEM of the threshold switch device and memristor device, while Fig. 10.14B shows the measured *I-V* characteristics. The presence of the select device successfully suppresses the leakage current at the half read region.

Bricalli et al. reported Ag/Silicon oxide-based ($Ag/SiO_x/C$) selector device which shows stable switching voltage ($+V_{th} \approx 2$ and $-V_{th} \approx -0.5$ V) and $I_{OFF} \approx 1$ pA under cycling, as shown in Fig. 10.15A [60]. They also characterized 1S1R structures by serially connecting the $Ag/SiO_x/C$ threshold switch with a discrete $Ti/SiO_x/C$ RRAM device. Fig. 10.15B shows the measured *I-V* characteristics of 1S1R device. The leakage current was significantly suppressed at the half read region.

As shown above, the CBRAM-type selector devices have shown excellent properties such as ultralow leakage current and sharp transition. Since the switching (formation and rupture of an Ag or Cu filament) occurs without causing electrical break-down of the dielectric, the low $I_{OFF}$ can be maintained under cycling. Also, the abrupt transition is attributed to the filamentary mechanism.

However, the CBRAM-type selector device lost TS characteristics and exhibit memory characteristics after electrical pulse with certain current compliance, due

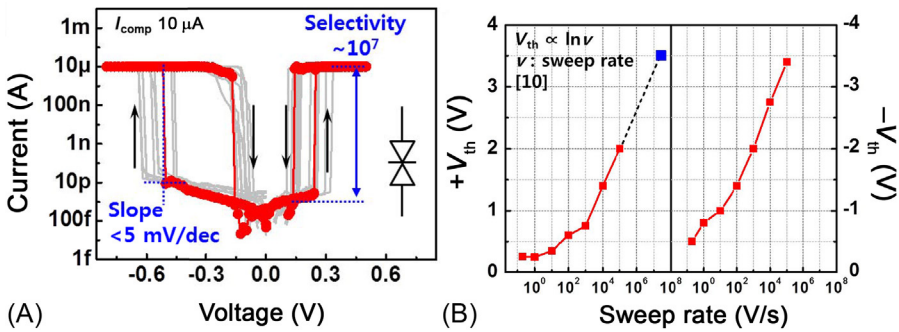


**Fig. 10.13** (A) *I-V* characteristics and (B) dependence of $V_{th}$ on voltage sweep rate of $Ag/TiO_2/Pt$ selector device.

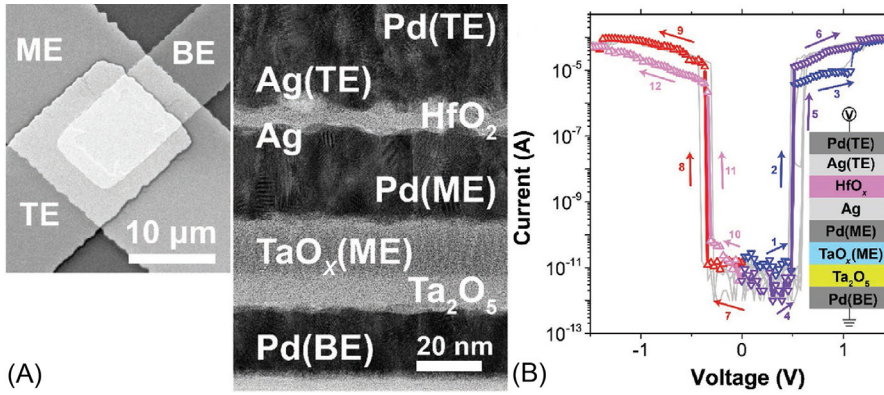


**Fig. 10.14** (A) Cross-sectional TEM image and (B) *I-V* characteristics of an integrated 1S-1R device consisting of a Pd/Ag/$HfO_x$/Ag/Pd selector and a Pd/$Ta_2O_5$/$TaO_x$/Pd memristor.

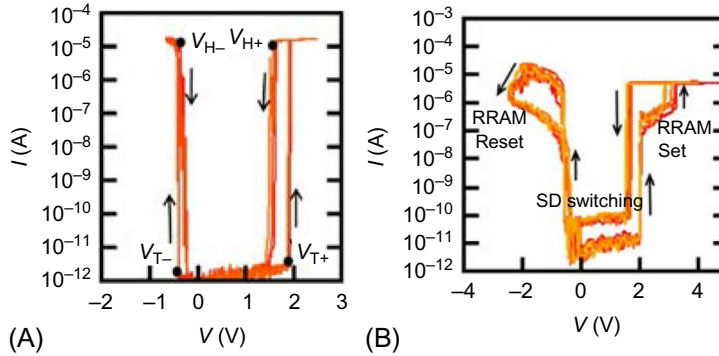


**Fig. 10.15** (A) *I-V* characteristics of an Ag/$SiO_x$-based (Ag/$SiO_x$/C) selector device and (B) 1S-1R device consisting of a Ag/$SiO_x$/C selector and a Ti/$SiO_x$/C RRAM.

to relatively thick filament formation. The maximum on-current of Ag/$TiO_2$/Pt [55], Pd/Ag/$HfO_x$/Ag/Pd [58], and Ag/$SiO_x$/C [60] selector devices are 10, 100, and 80 μA, respectively.

Also, the operation of the CBRAM-type selector device is based on the ionic motion [61], the switching speed is slower than the electronic-based systems such as IMT and OTS devices. The turn-on operation is performed by applying a voltage. Therefore, the turn-on (delay and transition) speed can be boosted by increasing applied voltage due to the exponential relation between time and voltage (Fig. 10.13B) and a delay speed of less than 75 ns [58] and a transition speed of less than 10 ns [55] have been reported. However, the turn-off (relaxation) speed is slower than the turn-on speed because it has a self-rupturing mechanism without an applied voltage. The Ag/$TiO_2$/Pt selector device can switch to the off-state when time delay is more than 1 μs after turn-on operation but it remains on on-state when time delay is less than 500 ns [62]. The Pd/Ag/$HfO_x$/Ag/Pd selector device shows turn off (relaxation) speed of 250 ns [58].

Therefore, the further research efforts are needed to improve the maximum on-current and relaxation speed of CBRAM-type selector device.

Song et al. proposed the AgTe/$TiO_2$/Pt stack to maintain selector characteristics with fast filament dissolution under high on-current stress [63]. The Te allows an extraction of Ag out of the switching layer because Ag tends to form Ag-Te phases which are more favorable [64, 65]. Therefore, the moderate Te content (35% Te) can acts as an additional driving force for fast filament dissolution which shows the TS behavior even at high operation current (Fig. 10.16A). In addition, the selector device with AgTe TE (AgTe/$TiO_2$/Pt) shows turn off (relaxation) speed of 100 ns which is 10 times faster than that of selector device with Ag TE (Ag/$TiO_2$/Pt). The enhanced on-current and relaxation speed were attributed to the formation of Ag-Te phase which accelerates the filament dissolution.

Zhao et al. obtained selector (Ag/defective-grain/$SiO_2$/Pt) with very high on-current (500 μA) and fast on/off switching speed (<0.1/1 μs) by introducing defective graphene (DG) layer between active electrode and switching layer, as shown in Fig. 10.17 [66]. They fabricated discrete graphene defects with various concentrations/sizes by irradiation of accelerated $Si^+$ ions. The cation injecting path to the switching layer is modulated by the discrete atomic-scale graphene defects and it results in the formation of discrete tiny conductive filaments which can be easily spontaneous ruptured.

In order to improve the performance of CBRAM-type selector device, various attempts have been made such as utilizing AgTe alloy electrode or DG layer. However, as described earlier, the different selector performances are exhibited in various materials. Therefore, in-depth study of the switching mechanism of the selector device is essential to provide guidelines for improving selector performance. The turn-on operation is the same as the conventional CBRAM device. The turn-on process occurs when a sufficient positive voltage is applied to the active electrode. The overall process involves the following steps: (i) anodic dissolution of the active electrode; (ii) migration of metal cations in the switching layer electrode under the external electric field; and (iii) reduction of metal cations and growth of the metal filaments from the counter electrode [61]. In the case of a turn-off operation in which the filament

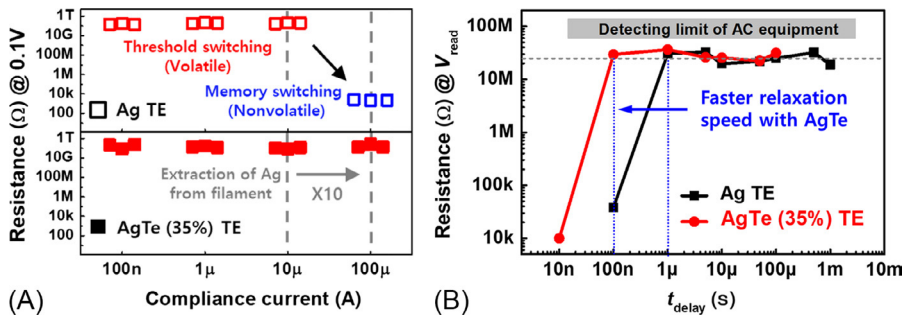


**Fig. 10.16** (A) Read resistance following turn-on operation with increasing compliance current and (B) measured relaxation speed of selector devices with Ag TE and AgTe (35%) TE.

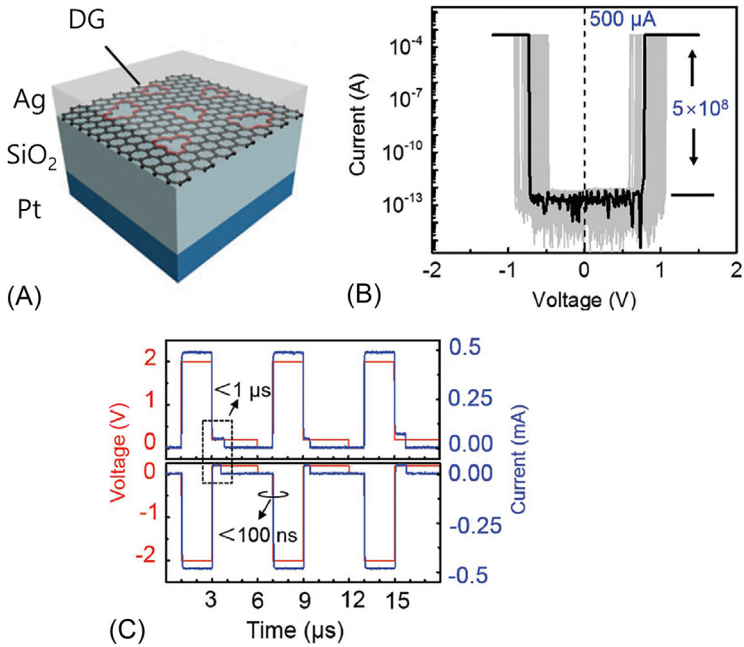


**Fig. 10.17** (A) Schematic illustrations and (B) *I-V* characteristics and switching speed of an Ag/defective-grain/$SiO_2$/Pt selector device.

ruptures when the applied voltage is removed, the mechanism has not yet been established, but various attempts have been made to understand it.

Hsiung et al. reported the volatile characteristics of Ag/$TiO_2$/Pt cell and observed the filament breaks up into a chain of nanospheres [54]. They explained the phenomena by using Rayleigh instability theorem, or so-called Thomas-Gibbs theorem. Wang et al. also observed spontaneous formation of Ag particles to minimize interfacial energy between Ag and the dielectric in a planar Au/$SiO_xN_y$:Ag/Au device when removing the electrical biasing after forming a continuous Ag filament [53]. Ambrogio et al. reported that the ion migration-induced mechanical stress affects ion hopping in two migration directions, therefore leading to switching asymmetry and even spontaneous CF dissolution in Ag/$GeS_2$/W system [48].

In addition, various mechanisms such as steric repulsion [55], electromotive force [47], and tunneling barrier modulation [59] have been proposed. However, this mechanism only qualitatively explains why the filaments are broken in each material. Therefore, quantitative studies based on physical evidence are needed to find out which parameters of the material determine the selector properties.

Recently, Shukla et al. conducted a quantitative analysis based on the first principle calculations on the effect of the energy difference (between the cluster configuration in the high-resistance state, and the filament configuration in the low-resistance state) on the selector characteristics, as shown in Fig. 10.18 [67]. The larger the energy difference value, the stronger the force to break the filament.

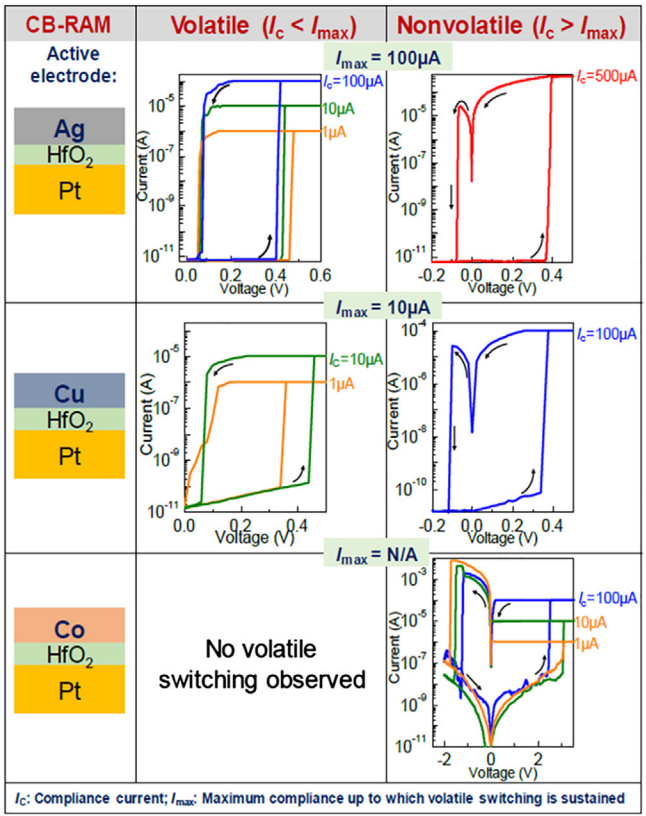


(A)

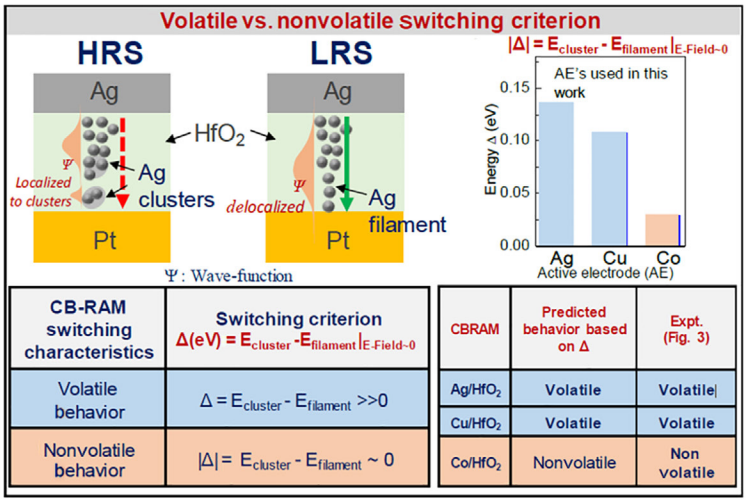


(B)

**Fig. 10.18** (A) Experimental switching characteristics for various active electrodes and (B) criterion for volatile vs nonvolatile switching.

The calculated energy difference values of Ag and Cu are 0.1354 and 0.1076 eV, respectively. This is consistent with the fact that most of the reported CBRAM-type selectors are Ag-based and Ag-based selectors show a higher maximum current than Cu-based selectors.

## 10.5 Conclusion

In this chapter, we demonstrate a selector device to compensate for the limitations of the two-terminal emerging memories to implement an ultrahigh-density crossbar arrays. The crossbar array consists of emerging memories suffers from undesired data disturbance and current flow. To minimize undesirable characteristics without changing the intrinsic operating characteristics of the memory device, there are various requirements of the selector device related with electrical characteristics (low OFF current, high ON-current density, fast switching speeds, infinite cycling endurance, large voltage margins, and compatible operating voltage conditions with storage devices) and fabrication process (low-temperature fabrication processes, high thermal stability, 3D stackable, and two-terminal device structure).

Though various candidates for the selector devices have been reported to replace conventional switch elements (CMOS transistor and P-N diode, etc.), we tried to demonstrate the researches about threshold-type selector devices such as IMT, OTS, and CBRAM-type devices due to their potential for atomic scale scalability.

The selector device with IMT behaviors has been widely researched based on excellent electrical characteristics and fabrication process compatibility. However, IMT device suffers from high OFF current problem because the metal and insulator phase are separated by very small electronic energy difference. Nevertheless, various studies have been conducted to reduce OFF current by suppressing the leakage path in insulators using additional barrier layers.

Recently, the OTS selector devices have shown the ideal selector characteristics of the crossbar array architecture. Especially, the simple binary-composition OTS have overcome the fabrication complexity which was critical bottleneck for the OTS selector. However, further enhancement of reliability issues such as cell-to-cell or cycle-to-cycle uniformity and thermal stability must be implemented based on understanding the switching mechanisms.

The CBRAM-type selector devices exhibit excellent nonlinear *I-V* characteristics. However, it exhibits slow turn OFF speed and even loss of selector characteristics at high operating current conditions. Therefore, to improve the switching speed, many research groups have studied the origin of filament instability based on their hypothesis and provided guidelines for ideal selector characteristics.

Nonidealities of the crossbar array architecture hinder the implementation of ultradense storage systems. However, the development of an ideal selector with insight into the switch mechanism will lead to overcoming the problems of crossbar arrays and the scaling limit of conventional memory technologies.

## References


[1] E.P.G. Wright, Electric connecting device, U.S. patent 2 667 542, Sept. 25, 1954.

[2] D. Kau, T. Stephen, I.V. Karpov, R. Dodge, B. Klehn, J.A. Kalb, J. Strand, A. Diaz, N. Leung, J. Wu, S. Lee, T. Langtry, K. Chang, C. Papagianni, J. Lee, J. Hirst, S. Erra, E. Flores, N. Righos, H. Castro, G. Spadini, A stackable cross point phase change memory, in: Proc. IEEE Int. Electron Devices Meeting, Dec. 2009, pp. 27.1.1–27.1.4.

[3] R. Waser, R. Dittmann, G. Staikov, K. Szot, Redox-based resistive switching memories—nanoionic mechanisms, prospects, and challenges, Adv. Mater. 21 (Jul. 2009) 2632–2663.

[4] G.W. Burr, R.S. Shenoy, K. Virwani, P. Narayanan, A. Padilla, B. Kurdi, H. Hwang, Access devices for 3D crosspoint memory, J. Vac. Sci. Technol. 32 (4) (Jun. 2014) 040802.

[5] A. Zylbersztejn, N.F. Mott, Metal-insulator transition in vanadium dioxide, Phys. Rev. B 11 (11) (Jun. 1975) 4383.

[6] V. Eyert, The metal-insulator transition of $NbO_2$: an embedded Peierls instability, Europhys. Lett. 58 (6) (Apr. 2002) 851.

[7] F.J. Morin, Oxides which show a metal-to-insulator transition at the Neel temperature, Phys. Rev. Lett. 3 (1) (Jul. 1959) 34.

[8] A. Cavalleri, M. Rini, H.H.W. Chong, S. Fourmaux, T.E. Glover, P.A. Heimann, J.C. Kieffer, R.W. Schoenlein, Band-selective measurements of electron dynamics in VO2 using femtosecond near-edge X-ray absorption, Phys. Rev. Lett. 95 (6) (Aug. 2005) 067405.

[9] M. Son, J. Lee, J. Park, J. Shin, G. Chio, S. Jung, W. Lee, S. Kim, S. Park, H. Hwang, Excellent selector characteristics of nanoscale $VO_2$ for high-density bipolar ReRAM applications, IEEE Electron Device Lett. 32 (11) (Nov. 2011) 1579–1581.

[10] J. Wei, Z. Wang, W. Chen, D.H. Cobden, New aspects of the metal-insulator transition in single-domain vanadium dioxide nanobeams, Nat. Nanotechnol. 4 (May 2009) 420–424.

[11] E. Cha, J. Woo, D. Lee, et al., Nanoscale (~10nm) 3D vertical ReRAM and $NbO_2$ threshold selector with TiN electrode, in: Proc. IEEE Int. Electron Devices Meeting, Dec. 2013, pp. 10.5.1–10.5.4.

[12] M. Son, J. Lee, J. Park, J. Shin, G. Choi, S. Jung, W. Lee, S. Kim, S. Park, H. Hwang, Excellent selector characteristics of nanoscale $VO_2$ for high-density bipolar ReRAM applications, IEEE Electron Device Lett. 32 (11) (Aug. 2011) 1579–1581.

[13] S. Kumar, M.D. Pickett, J.P. Strachan, G. Gibson, Y. Nishi, R.S. Williams, Local temperature redistribution and structural transition during joule-heating-driven conductance switching in $VO_2$, Adv. Mater. 25 (42) (Nov. 2013) 6128–6132.

[14] W.A. Vitale, E.A. Casu, A. Biswas, T. Rosca, C. Alper, A. Krammer, G.V. Luong, Q.T. Zhao, S. Mantl, A. Schuler, A.M. Ionescu, A steep-slope transistor combining phase-change and band-to-band-tunneling to achieve a sub-unity body factor, Sci. Rep. 7 (355) (Feb. 2017) 1–10.

[15] S. Kim, X. Liu, J. Park, S. Jung, W. Lee, J. Woo, J. Shin, G. Choi, C. Cho, S. Park, D. Lee, E. Cha, B. Lee, H. Lee, S. Kim, S. Jung, H. Hwang, Ultrathin (<10nm) $Nb_2O_5/NbO_2$ hybrid memory with both memory and selector characteristics for high density 3D vertically stackable RRAM applications, in: Symposium on VLSI Technology, 2012, pp. T18.3.

[16] X. Liu, S.M. Sadaf, M. Son, J. Shin, J. Park, J. Lee, S. Park, H. Hwang, Diode-less bilayer oxide ($WO_x$-$NbO_x$) device for cross-point resistive memory applications, Nanotechnology 22 (47) (Nov. 2011) 175702.

[17] E. Cha, J. Park, J. Woo, D. Lee, A. Prakash, H. Hwang, Comprehensive scaling study of $NbO_2$ insulator-metal-transition selector for cross point array application, Appl. Phys. Lett. 108 (15) (Apr. 2016) 153502.

[18] S.K. Nandi, X. Liu, D.K. Venkatachalam, R.G. Eliman, Threshold current reduction for the metal-insulator transition in $NbO_{2-x}$-selector devices: the effect of ReRAM integration, J. Phys. D 48 (19) (Apr. 2015) 195105.

[19] X. Liu, S. Md, M. Son, J. Park, J. Shin, W. Lee, K. Seo, D. Lee, H. Hwang, Co-occurrence of threshold switching and memory switching in Pt/$NbO_x$/Pt cells for crosspoint memory applications, IEEE Electron Device Lett. 33 (2) (Feb. 2012) 236–238.

[20] C. Funck, S. Menzel, N. Aslam, H. Zhang, A. Hardtdegen, R. Waser, S.H. Eifert, Multidimensional simulation of threshold switching in $NbO_2$ based on an electric field triggered thermal runaway model, Adv. Electron. Mater. 2 (7) (Jun. 2016) 201600169.

[21] S. Slesazeck, H. Mähne, H. Wylezich, A. Wachowiak, J. Radhakrishnan, A. Ascoli, R. Tetzlaff, T. Mikolajick, Physical model of threshold switching in $NbO_2$ based memristors, RSC Adv. 5 (124) (Nov. 2015) 102318–102322.

[22] G.A. Gibson, S. Musunuru, J. Zhang, K. Vandenberghe, J. Lee, C.C. Hsieh, W. Jackson, Y. Jeon, D. Henze, Z. Li, S. Williams, An accurate locally active memristor model for S-type negative differential resistance in $NbO_x$, Appl. Phys. Lett. 108 (2) (Jan. 2016) 023505.

[23] J. Park, E. Cha, I. Karpov, H. Hwang, Dynamics of electroforming and electrically driven insulator-metal transition in $NbO_2$ selector, Appl. Phys. Lett. 108 (23) (Jun. 2016) 232101.

[24] J. Park, E. Cha, D. Lee, S. Lee, J. Song, J. Park, H. Hwang, Improved threshold switching characteristics of multi-layer $NbO_x$ for 3-D selector application, Microelectron. Eng. 147 (Apr. 2015) 318–320.

[25] G. Bersukera, J. Yum, L. Vandelli, A. Padovani, L. Larcher, V. Iglesias, M. Porti, M. Nafría, K. McKenna, A. Shluger, P. Kirsch, R. Jammy, Grain boundary-driven leakage path formation in $HfO_2$ dielectrics, Solid State Electron. 65–66 (Jul. 2011) 146–150.

[26] J. Park, T. Hadamek, A.B. Posadas, E. Cha, A.A. Demkov, H. Hwang, Multi-layered $NiO_y$/$NbO_x$/$NiO_y$ fast drift-free threshold switch with high Ion/Ioff ratio for selector application, Sci. Rep. 7 (Jun. 2017) 4068.

[27] X. Liu, S.K. Nandi, D.K. Venkatachalam, K. Belay, S. Song, R.G. Elliman, Reduced threshold current in $NbO_2$ selector by engineering device structure, IEEE Electron Device Lett. 35 (10) (Aug. 2014) 1055–1057.

[28] S.R. Ovshinsky, Reversible electrical switching phenomena in disordered structures, Phys. Rev. Lett. 21 (20) (Nov. 1968) 1450–1453.

[29] Y. Koo, K. Baek, H. Hwang, Te-based amorphous binary OTS device with excellent selector characteristics for X-point memory applications, in: Symp. VLSI Tech. Dig, Jun. 2016, pp. T86–T87.

[30] S. Yasuda, K. Ohba, T. Mizuguchi, H. Sei, M. Shimuta, K. Aratani, T. Shiimoto, T. Yamamoto, T. Sone, S. Nonoguchi, J. Okuno, A. Kouchiyama, W. Otsuka, K. Tzutsui, A cross point Cu-ReRAM with a novel OTS selector for storage class memory applications, in: Symp. VLSI Tech. Dig, Jun. 2017, pp. T30–T31.

[31] M. Lee, D. Lee, H. Kim, H. Choi, J. Park, H. Kim, Y. Cha, U. Chung, I. Yoo, K. Kim, Highly-scalable threshold switching select device based on chalcogenide glasses for 3D nanoscaled memory arrays, in: Proc. IEEE Int. Electron Devices Meeting, Dec. 2012, pp. 2.6.1–2.6.3.

[32] S.R. Ovshinsky, An introduction to ovonic research, J. Non-Cryst. Solids 2 (1970) 99–106.

[33] H.Y. Cheng, W.C. Chien, I.T. Kuo, E.K. Lai, Y. Zhu, J.L. Jordan-Sweet, A. Ray, F. Carta, F.M. Lee, P.H. Tseng, M.H. Lee, Y.Y. Lin, W. Kim, R. Bruce, C.W. Yeh, C.H. Yang, M. BrightSky, H.L. Lung, An ultra high endurance and thermally stable selector based on TeAsGeSiSe chalcogenides compatible with BEOL IC integration for cross-point PCM, in: Proc. IEEE Int. Electron Devices Meeting, Dec. 2017, pp. 2.2.1–2.2.4.

[34] Y. Koo, S. Lee, S. Park, M. Yang, H. Hwang, Simple binary ovonic threshold switching material SiTe and its excellent selector performance for high-density memory array application, IEEE Electron Device Lett. 38 (5) (May 2017) 568–571.
[35] S. Kim, H. Kim, S. Choi, Intrinsic threshold switching responses in AsTeSi thin film, J. Alloys Compd. 667 (Jan. 2016) 91–95.
[36] A.C. Warren, Reversible thermal breakdown as a switching mechanism in chalcogenide glasses, IEEE Trans. Electron Devices 20 (2) (1973) 123–131.
[37] D. Adler, M.S. Shur, M. Silver, S.R. Ovshinsky, Threshold switching in chalcogenide-glass thin films, J. Appl. Phys. 51 (6) (Jun. 1980) 3289–3309.
[38] A. Pirovano, A.L. Lacaita, A. Benvenuti, F. Pellizzer, R. Bez, Electronic switching in phase-change memories, IEEE Trans. Electron Devices 51 (3) (Mar. 2004) 452–459.
[39] D. Emin, Current-driven threshold switching of a small polaron semiconductor to a metastable conductor, Phys. Rev. B 74 (3) (2006) 035206.
[40] M. Nardone, V.G. Karpov, D.C.S. Jackson, I.V. Karpov, A unified model of nucleation switching, Appl. Phys. Lett. 94 (2009) 103509.
[41] D. Ielmini, Threshold switching mechanism by high-field energy gain in the hopping transport of chalcogenide glasses, Phys. Rev. B 78 (3) (2008) 035308.
[42] B. Govoreanu, G.L. Donadio, K. Opsomer, W. Devulder, V.V. Afanas'ev, T. Witters, S. Clima, N.S. Avasarala, A. Redolfi, S. Kundu, O. Richard, D. Tsvetanova, G. Pourtois, C. Detavernier, L. Goux, G.S. Kar, Thermally stable integrated Se-based OTS selectors with >20 MA/cm$^2$ current drive, >3.10$^3$ half-bias nonlinearity, tunable threshold voltage and excellent endurance, in: Symp. VLSI Tech. Dig, Jun. 2017, pp. T92–T93.
[43] S. Clima, B. Govoreanu, K. Opsomer, A. Velea, N.S. Avasarala, W. Devulder, I. Shlyakhov, G.L. Donadio, T. Witters, S. Kundu, L. Goux, V. Afanasiev, G.S. Kar, G. Pourtois, Atomistic investigation of the electronic structure, thermal properties and conduction defects in Ge-rich $Ge_xSe_{1-x}$ materials for selector applications, in: Proc. IEEE Int. Electron Devices Meeting, Dec. 2017, pp. 4.1.1–4.1.4.
[44] A. Verdy, G. Navarro, V. Sousa, P. Noé, M. Bernard, F. Fillot, G. Bourgeois, J. Garrione, L. Perniola, Improved electrical performance thanks to Sb and N doping in Se-rich GeSe-based OTS selector devices, in: IEEE International Memory Workshop (IMW), May 2017.
[45] F. Rao, Z. Song, Y. Cheng, M. Xia, K. Ren, L. Wu, B. Liu, S. Feng, Investigation of changes in band gap and density of localized states on phase transition for $Ge_2Sb_2Te_5$ and $Si_{3.5}Sb_2Te_3$ materials, Acta Mater. 60 (2012) 323–328.
[46] J. Lee, G. Kim, Y. Ahn, J. Park, S. Ryu, C. Hwang, H. Kim, Threshold switching in Si-As-Te thin film for the selector device of crossbar resistive memory, Appl. Phys. Lett. 100 (Mar. 2012) 123505.
[47] J.V.D. Hurk, E. Linn, H. Zhang, R. Waser, I. Valov, Volatile resistance states in electrochemical metallization cells enabling non-destructive readout of complementary resistive switches, Nanotechnology 25 (42) (Sep. 2014) 425202.
[48] S. Ambrogio, S. Balatti, S. Choi, D. Ielmini, Impact of the mechanical stress on switching characteristics of electrochemical resistive memory, Adv. Mater. 26 (23) (2014) 3885–3892.
[49] J. Song, A. Prakash, D. Lee, J. Woo, E. Cha, S. Lee, H. Hwang, Bidirectional threshold switching in engineered multilayer ($Cu_2O$/Ag:$Cu_2O$/$Cu_2O$) stack for cross-point selector application, Appl. Phys. Lett. 107 (11) (Sep. 2015) 113504.
[50] Q. Luo, X. Xu, H. Liu, H. Lv, T. Gong, S. Long, Q. Liu, H. Sun, W. Banerjee, L. Li, N. Lu, M. Liu, Cu BEOL compatible selector with high selectivity (>10$^7$), extremely low off-current (~pA) and high endurance (>10$^{10}$), in: Proc. IEEE IEDM, Dec. 2015, pp. 10.4.1–10.4.4.

[51] W. Chen, H.J. Barnaby, M.N. Kozicki, Volatile and non-volatile switching in Cu-$SiO_2$ programmable metallization cells, IEEE Electron Device Lett. 37 (5) (2016) 580–583.

[52] J. Woo, D. Lee, E. Cha, S. Lee, S. Park, H. Hwang, Control of Cu conductive filament in complementary atom switch for cross-point selector device application, IEEE Electron Device Lett. 35 (1) (Jan. 2014) 60–62.

[53] Z. Wang, S. Joshi, S.E. Saveliev, H. Jiang, R. Midya, P. Lin, M. Hu, N. Ge, J.P. Strachan, Z. Li, Q. Wu, M. Barnell, G.-L. Li, H.L. Xin, R.S. Williams, Q. Xia, J.J. Yang, Memristors with diffusive dynamics as synaptic emulators for neuromorphic computing, Nat. Mater. 16 (1) (2017) 101–108.

[54] C.-P. Hsiung, H.-W. Liao, J.-Y. Gan, T.-B. Wu, J.-C. Hwang, F. Chen, M.-J. Tsai, Formation and instability of silver nanofilament in Ag-based programmable metallization cells, ACS Nano 4 (9) (2010) 5414–5420.

[55] J. Song, J. Woo, A. Prakash, D. Lee, H. Hwang, Threshold selector with high selectivity and steep slope for cross-point memory array, IEEE Electron Device Lett. 36 (7) (Jul. 2015) 681–683.

[56] J. Yoo, J. Woo, J. Song, H. Hwang, Threshold switching behavior of Ag-Si based selector device and hydrogen doping effect on its characteristics, AIP Adv. 5 (12) (Dec. 2015) 127221.

[57] N. Shukla, B. Grisafe, R.K. Ghosh, N. Jao, A. Aziz, J. Frougier, M. Jerry, S. Sonde, S. Rouvimov, T. Orlova, S. Gupta, S. Datta, Ag/$HfO_2$ based threshold switch with extreme non-linearity for unipolar cross-point memory and steep-slope Phase-FETs, in: Proc. IEEE IEDM, Dec. 2016, pp. 34.6.1–34.6.4.

[58] R. Midya, Z. Wang, J. Zhang, S.E. Savel'ev, C. Li, M. Rao, M.H. Jang, S. Joshi, H. Jiang, P. Lin, K. Norris, N. Ge, Q. Wu, M. Barnell, Z. Li, H.L. Xin, R.S. Williams, Q. Xia, J.J. Yang, Anatomy of Ag/hafnia-based selectors with $10^{10}$ nonlinearity, Adv. Mater. 29 (12) (Jan. 2017) 1604457.

[59] H. Sun, Q. Liu, C. Li, S. Long, H. Lv, C. Bi, Z. Huo, L. Li, M. Liu, Direct observation of conversion between threshold switching and memory switching induced by conductive filament morphology, Adv. Funct. Mater. 24 (36) (2014) 5679–5686.

[60] A. Bricalli, E. Ambrosi, M. Laudato, M. Maestro, R. Rodriguez, D. Ielmini, $SiO_x$-based resistive switching memory (RRAM) for crossbar storage/select elements with high on/off ratio, in: Proc. IEEE IEDM, Dec. 2016, pp. 4.3.1–4.3.4.

[61] I. Valov, R. Waser, J.R. Jameson, M.N. Kozicki, Electrochemical metallization memories–fundamentals, applications, prospects, Nanotechnology 22 (25) (Jun. 2011) 254003.

[62] J. Song, J. Woo, S. Lee, A. Prakash, J. Yoo, K. Moon, H. Hwang, Steep slope field-effect transistors with Ag/TiO2-based threshold switching device, IEEE Electron Device Lett. 37 (7) (Jul. 2016) 932–934.

[63] J. Song, J. Park, K. Moon, J. Woo, S. Lim, J. Yoo, D. Lee, H. Hwang, Monolithic integration of AgTe/$TiO_2$ based threshold switching device with TiN liner for steep slope field-effect transistors, in: Proc. IEEE IEDM, Dec. 2016, pp. 25.3.1–25.3.4.

[64] W. Devulder, K. Opsomer, J. Meersschaut, D. Deduytsche, M. Jurczak, L. Goux, C. Detavernier, Combinatorial study of Ag–Te thin films and their application as cation supply layer in CBRAM cells, ACS Comb. Sci. 17 (5) (2015) 334–430.

[65] L. Goux, K. Opsomer, R. Degraeve, R. Müller, C. Detavernier, D.J. Wouters, M. Jurczak, L. Altimime, J.A. Kittl, Influence of the Cu-Te composition and microstructure on the resistive switching of Cu-Te/$Al_2O_3$/Si cells, Appl. Phys. Lett. 99 (5) (Aug. 2011) 053502.

[66] X. Zhao, J. Ma, X. Xiao, Q. Liu, L. Shao, D. Chen, S. Liu, J. Niu, X. Zhang, Y. Wang, R. Cao, W. Wang, Z. Di, H. Lv, S. Long, M. Liu, Breaking the current-retention dilemma in cation-based resistive switching devices utilizing graphene with controlled defects, Adv. Mater. (Feb. 2018) 1–9. 1705193.

[67] N. Shukla, R.K. Ghosh, B. Grisafe, S. Datta, Fundamental mechanism behind volatile and non-volatile switching in metallic conducting bridge RAM, in: Proc. IEEE IEDM, Dec. 2017, pp. 4.3.1–4.3.4.